



Inhibition of TAF1B impairs ribosome biosynthesis and suppresses cell proliferation in stomach adenocarcinoma through promoting c-MYC mRNA degradation

Hang-fei Chen^{a,b,1}, Zhang-ping Li^{c,1}, Qi Wu^a, Chun Yu^d, Jing-Yi Yan^e, Yong-feng Bai^a, Sheng-mei Zhu^a, Mao-xiang Qian^f, Ming Liu^a, Li-feng Xu^a, Zheng Peng^{g,**}, Feng Zhang^{a,b,*}

^a The Joint Innovation Center for Engineering in Medicine, the Quzhou Affiliated Hospital of Wenzhou Medical University, Quzhou People's Hospital, Quzhou 324000, China

^b The 2nd Clinical Medical College, Zhejiang Chinese Medical University, Hangzhou 310053, China

^c Department of Emergency Medicine, the Quzhou Affiliated Hospital of Wenzhou Medical University, Quzhou People's Hospital, Quzhou 324000, China

^d Department of Gastroenterology, the Quzhou Affiliated Hospital of Wenzhou Medical University, Quzhou People's Hospital, Quzhou 324000, China

^e The First Affiliated Hospital of Wenzhou Medical University, Wenzhou 325000, Zhejiang, China

^f Institute of Pediatrics and Department of Hematology and Oncology, National Children's Medical Center, Children's Hospital of Fudan University, Institutes of Biomedical Sciences, Fudan University, Shanghai 200032, China

^g Department of Radiation Oncology, the Quzhou Affiliated Hospital of Wenzhou Medical University, Quzhou People's Hospital, Quzhou 324000, China

ARTICLE INFO

Keywords:

TAF1B
Stomach adenocarcinoma
c-MYC
Nucleolar stress
Ribosome biosynthesis
RNA polymerase I

ABSTRACT

Hyperactivation of ribosome biosynthesis (RiBi) is a hallmark of cancer, and targeting ribosome biogenesis has emerged as a potential therapeutic strategy. The depletion of *TAF1B*, a major component of selectivity factor 1 (*SL1*), disrupts the pre-initiation complex, preventing RNA polymerase I from binding ribosomal DNA and inhibiting the hyperactivation of RiBi. Here, we investigate the role of *TAF1B*, in regulating RiBi and proliferation in stomach adenocarcinoma (STAD). We disclosed that the overexpression of *TAF1B* correlates with poor prognosis in STAD, and found that knocking down *TAF1B* effectively inhibits STAD cell proliferation and survival *in vitro* and *in vivo*. *TAF1B* knockdown may also induce nucleolar stress, and promote c-MYC degradation in STAD cells. Furthermore, we demonstrate that *TAF1B* depletion impairs rRNA gene transcription and processing, leading to reduced ribosome biogenesis. Collectively, our findings suggest that *TAF1B* may serve as a potential therapeutic target for STAD and highlight the importance of RiBi in cancer progression.

* Corresponding author. The Joint Innovation Center for Engineering in Medicine, the Quzhou Affiliated Hospital of Wenzhou Medical University, Quzhou People's Hospital, Quzhou 324000, China.

** Corresponding author.

E-mail addresses: hdpz@163.com (Z. Peng), fengzhang@wmu.edu.cn (F. Zhang).

¹ These authors contributed equally to this work.

<https://doi.org/10.1016/j.heliyon.2023.e23167>

Received 24 August 2023; Received in revised form 23 November 2023; Accepted 28 November 2023

Available online 1 December 2023

2405-8440/© 2023 The Authors. Published by Elsevier Ltd. This is an open access article under the CC BY-NC-ND license (<http://creativecommons.org/licenses/by-nc-nd/4.0/>).

1. Introduction

Stomach adenocarcinoma (STAD) is the fifth most common cancer worldwide and the third leading cause of cancer-related deaths [1]. STAD is associated with multiple risk factors, including *Helicobacter pylori* (Hp) infection, older age, and an unhealthy diet high in salt and low in fruit and vegetable consumption [2]. Hp infection was once considered the primary pathogenic factor of gastric cancer, however, its prevalence has decreased in recent decades due to improved sanitation and economic development [2]. Hp screening and eradication programs in Japan, South Korea, and other high-prevalence areas have significantly reduced gastric cancer-related mortality [3–5]. However, gastric cancer incidence is increasing among young people in high-income regions globally, regardless of Hp prevalence [6]. This suggests that other factors beyond Hp infection are contributing to rising gastric cancer rates.

Ribosome biosynthesis (RiBi) is one of the most prominent features of cell growth and proliferation [7]. It is also recognized as a hallmark of cancer and an emerging therapeutic target [7–10]. Clinical trials of small-molecule inhibitors of RiBi such as CX-5461 and BMH-21 are currently underway to selectively target tumor cells [11]. RiBi involves a complex series of processes, among which transcription of the precursor of ribosomal RNA (pre-rRNA) via RNA polymerase I (*PolI*) is the first critical step [12]. Given the low affinity of *PolI* for ribosomal DNA (rDNA) promoters, accurate recruitment of *PolI* before transcription initiation requires a specific pre-initiation complex (PIC) [13]. Mammalian *PolI* PIC includes selectivity factor 1 (*SL1*), *RRN3*, and upstream binding factor (*UBF*), of which *SL1* is essential and stabilizes the PIC structure. Interestingly, prior study has demonstrated that human *SL1* can direct *PolI* transcription even in the absence of *UBF* [14].

TAF1B, also known as TBP-associated factor 1B, constitutes a vital component of *SL1*, which recruits RNA polymerase I (*PolI*) for accurate transcription of ribosomal pre-rRNA. *TAF1B* facilitates *PolI* binding to the *SL1* complex by interacting with *RRN3* [15,16], and directly binds the rDNA promoter to promote *SL1* recruitment [17,18]. Furthermore, *TAF1B* can also influence the activity of *SL1* through post-recruitment of polymerase [19]. While *TAF1B* is essential for the pre-initiation complex of *PolI*, its specific role in cancer pathogenesis remains poorly understood. A study by Gupta et al. revealed a correlation between mutations in *TAF1B* and congenital pouch colon type IV, suggesting that the presence of missense or stop gain mutations in *TAF1B* may contribute to the aggressive nature of this condition [20]. Furthermore, inactivating mutations in *TAF1B* were found to be more prevalent in microsatellite-unstable colorectal cancer [21]. Our previous research also identified high expression of *TAF1B* in hepatocellular carcinoma (HCC) and its association with poor prognosis in HCC patients [22]. In light of these findings, our study aims to investigate the functional role of *TAF1B* in STAD.

2. Materials and methods

2.1. Patients and tissue samples

Tissue samples were gathered from patients with STAD who had undergone radical resection. Tumors and paired paracancerous tissues collected were used for immunohistochemical analysis. Each patient signed an informed consent form for sample collection.

2.2. Plasmids

The oligonucleotides encoding two short hairpin RNAs (shRNAs #2 and #6) targeting *TAF1B* were synthesized by Genewiz (Suzhou, China). The shRNA sequences were cloned into the pLKO.1 lentiviral vector. The target sequences of the shRNAs are shown in Table 1. The plasmid for c-Myc overexpression (Cat# HG11346-NY) was purchased from SinoBiological (Shanghai, China).

2.3. Antibodies

Antibodies targeting *TAF1B* (PA5-112,957), *TAF1D* (PA5-25509), and *RPL11* (#37–3000) were purchased from Thermo Fisher Scientific (Shanghai, China). Antibodies directed against TAF110 (TAFI C) (sc-374,551), TAF148 (TAFI A) (sc-393,600), and RPA135 (Pol I β) (sc-293,272) were obtained from Santa Cruz Biotechnology (Dallas, TX, USA). Antibodies specific to TAF12 (ab229487), TBP (ab818), c-MYC (ab32072), UBF (ab75781), *RRN3* (ab112052), Ki67 (ab15580, for immunofluorescence), TRBP (ab180947), Fibrillarin (ab5821) and Nucleophosmin (ab10530) were acquired from Abcam (Cambridge, UK). Antibodies against β -Actin (#3700), POLR1A (Pol I α) (#24799), p53 (#2524), Ki67 (#12202, for immunocytochemistry) and GAPDH (#2118) were obtained from Cell Signaling Technologies (Danvers, MA, USA).

2.4. Cell culture

HEK293T, GES-1, MKN-45, BGC-823, SGC-7901, MGC-803, and HGC-27 cell lines were procured from the American Type Culture

Table 1
The targeting sequences of shRNA.

Name	5'-3' sequences
shTAF1B RNA#2	GCAGGTGAGCTTCATTTGATT
shTAF1B RNA#6	GCAGGTGAGCTTCATTTGATT

Collection (Manassas, VA). The cells were cultured in Dulbecco's Modified Eagle Medium (DMEM, #8120448, Thermo Fisher Scientific, Shanghai, China) or RPMI1640 Medium (1640, #11875500, Thermo Fisher Scientific, Shanghai, China), supplemented with 10 % fetal bovine serum (FBS, #2148200RP, Gibco, Shanghai, China) in a humidified chamber with 5 % CO₂ at 37 °C.

2.5. Lentivirus production and transduction

Lentivirus production and transduction methods were carried out as previously reported. Briefly, shRNAs or cDNA plasmids were mixed with psPAX2 and pMD2.G plasmids and co-transfected into 293T cells with 80–90 % confluence in a 6-well plate using Lipofectamine 3000 reagent (#L3000015, Thermo Fisher Scientific, Shanghai, China) to generate lentiviral particles for gene transduction. Virus-containing supernatant was collected and centrifuged at 300g for 5 min to eliminate suspended 293T cells 48 h after transfection. The supernatants were mixed with polybrene at a final concentration of 10 µg/mL for infection of target cells. Cells were selected by 10 µg/mL puromycin for 3 days 24 h post-transduction and used for subsequent experiments.

2.6. Immunohistochemical staining and AgNOR

Immunohistochemical staining of paraffin-embedded sections (4 µm thick) was conducted as follows: sections were deparaffinized using xylene, and subjected to rehydration with decreasing concentrations of ethanol. Subsequently, tissue sections were incubated in 10 mmol/L citrate buffer (pH 6.0) and heated in a microwave oven for 15 min for antigen retrieval. To block endogenous peroxidase activity, the tissue sections were treated with 3 % hydrogen peroxide in PBS for 10 min. Thereafter, the sections were blocked with 5 % goat serum for 30 min and incubated with the primary antibodies overnight at 4 °C. Signal development was performed using the MaxVision™ HRP-Polymer IHC Kit (MXB Biotechnologies, Fuzhou, China) and nuclear counterstaining was achieved via hematoxylin staining. AgNOR staining was performed using paraffin-embedded sections (4 µm thick) that were deparaffinized with xylene, rehydrated with decreasing concentrations of ethanol, and washed in water for 10 min. Sections were then processed with AgNOR Stain solution (G2015, Solarbio, Beijing, China) at room temperature in the dark for 60 min. Subsequently, the tissue sections were dehydrated with increasing concentrations of ethanol and fixed with xylene and observed under a microscope. ImageJ (National Institutes of Health, Bethesda, MD) was used to perform quantitation.

2.7. Western blotting

Cells were collected and lysed using 1 × SDS buffer supplemented with phenylmethylsulfonyl fluoride (PMSF) and phosphatase inhibitors. The cell lysates were boiled for 10 min and centrifuged at 16,000 g for 10 min at 4 °C to remove cellular debris. SDS-PAGE was used to separate the proteins, which were then transferred to PVDF membranes. Following blocking with 0.1 % casein at room temperature for 1 h, the membranes were incubated with primary antibodies overnight at 4 °C. Subsequently, the membranes were blotted with HRP-conjugated secondary antibodies for 1 h at room temperature. Chemiluminescent signals were acquired using the Tanon 4200SF system (Tanon Biotechnology, Shanghai, China).

2.8. Colony formation assay

Cells from each group, as indicated by treatment, were in the logarithmic growth phase and were digested with 0.25 % Trypsin-EDTA (25200072, Gibco, Shanghai, China) to make a single-cell suspension. Each well of a 6-well plate was seeded with 500 cells. The cells were cultured for 14 days and the medium was changed every 3 days. Colonies in plates were stained with crystal violet solution (C0121-100 ml, Beyotime, Shanghai, China) for 15 min, and then washed with water to diminish background staining. Finally, images of the colonies were captured using an iPhone camera, and the numbers and diameters of clones were calculated using ImageJ software (National Institutes of Health, Bethesda, MD).

2.9. Immunofluorescent staining

To conduct immunofluorescent staining, the cells were fixed in a 4 % paraformaldehyde suspension and spun onto slides. Then, they were permeabilized with 0.5 % PBS-Triton X-100 for 10 min and blocked with 5 % goat serum for 1 h. Subsequently, the slides were incubated overnight with the indicated antibodies at 4 °C, followed by the appropriate secondary antibody, either 488 conjugated goat anti-mouse IgG (ab150120, Abcam, Cambridge, UK) or 594 conjugated goat anti-mouse IgG (ab150077, Abcam, Cambridge, UK). The slides were mounted in an Anti-fade Reagent with DAPI (#8961, Cell Signaling Technologies, Danvers, MA, USA) and analyzed using microscopy.

2.10. EdU Cell Proliferation Assay

To conduct the EdU Cell Proliferation Assay, gastric cancer cells were treated with the BeyoClick™ EdU Cell Proliferation Kit with Alexa Fluor 488 (C0071S, Beyotime, Shanghai, China) following the manufacturer's instructions. Briefly, the EdU working solution was added to a 6-well plate, and the cells were cultured for 2 h. The cells were then fixed in a 4 % paraformaldehyde suspension for 20 min and spun onto slides. Subsequently, the cells were permeabilized with 0.5 % PBS-Triton X-100 for 10 min, washed three times, and treated with 0.5 ml of Click reaction solution per well for 30 min at room temperature in the dark. The slides were then washed three

times with washing solution and mounted in Antifade Reagent with DAPI (#8961, Cell Signaling Technologies, Danvers, MA, USA) for microscopy analysis.

2.11. Cell cycle determination by flow cytometry

To determine the cell cycle, 1×10^6 cells were collected and resuspended in 50 μ L of cold PBS to produce a single-cell suspension. The cells were then fixed with 75 % cold ethanol overnight at 4 °C. The fixed cells were centrifuged at 100 g for 10 min before being washed with cold PBS three times. The cells were treated with RNase A (RT405-12, Tiangen, Beijing, China) at 37 °C for 30 min and stained with PI (S19136-10 mg, Yuanye Bio-Technology, Shanghai, China) at a final concentration of 50 μ g/ 10^6 cells. The stained cells were examined by flow cytometry (FC-500, Beckman Coulter, Brea, CA) and analyzed using ModFit LT software (Verity Software House, Topsham, ME).

2.12. Co-immunoprecipitation

For co-immunoprecipitation, gastric cancer cells were treated with Pierce™ Classic Magnetic IP/Co-IP Kit (#88804, Thermo Fisher Scientific, Shanghai, China) according to the manufacturer's instructions. Briefly, the medium was removed carefully and the cells were washed with cold PBS. IP Lysis buffer was then added to the cells, which were then incubated on ice for 5 min with periodic mixing. The resulting lysate was transferred to a microcentrifuge tube and centrifuged at $\sim 13,000 \times g$ for 10 min to pellet the cell debris. The cell lysate was combined with 2–10 μ g of IP antibody per sample in a microcentrifuge tube and incubated overnight at 4 °C to form the immune complex. Pre-washed magnetic beads were added, and the mixture was incubated at room temperature for 1 h while being mixed. The beads were collected with a magnetic stand, and the complex was washed three times. Next, 100 μ L of Elution Buffer was added to elute the immune complex, which was then mixed with Lane Marker Sample Buffer and analyzed by western blotting with the indicated antibodies.

2.13. Chromatin immunoprecipitation (ChIP) and ChIP-PCR

To conduct ChIP and ChIP-PCR, SGC-7901 cells were treated with 1 % formaldehyde for 10 min for chromatin crosslinking and subsequently with glycine for 5 min to neutralize the reaction. The cells were then washed with cold PBS and collected on ice (5×10^6 /mL). Chromatin acquisition was performed using the SimpleChIP® Enzymatic Chromatin IP Kit (Magnetic Beads) (#9003, Cell Signaling Technology, Danvers, MA, USA), and chromatin was immunoprecipitated at 4 °C overnight with the indicated antibodies according to the manufacturer's instructions. The immunoprecipitated products were collected after overnight incubation, and the beads were washed, eluted, and centrifuged. RNA was then digested using RNase and proteinase K. After DNA purification, the binding site was evaluated using qPCR with the Roche LightCyclerR 480 Quantitative PCR System (Indianapolis, IN, USA). The qRT-PCR primers are noted in Table 2.

2.14. EU nascent RNA detection

EU (ST2055-50 mg, Beyotime, Shanghai, China) was added to the complete culture medium from a 100 mM stock in DMSO. Gastric cancer cells were cultured with EU for 6 h. The cells were then fixed for 20 min in a 4 % paraformaldehyde suspension and permeabilized with 0.5 % PBS-Triton X-100 for 10 min. The cells were rinsed with TBST and stained for 30 min at room temperature with 100 mM Tris, pH 8.5/1 mM CuSO₄/10-50 μ M fluorescent azide (F278701-5 mg, Aladdin, Shanghai, China)/100 mM ascorbic acid (added last from a 0.5 M stock in water). After staining, the cells were washed several times with TBST and then mounted in Antifade Reagent with DAPI (#8961, Cell Signaling Technologies, Danvers, MA, USA) for imaging under a microscope.

2.15. Real-time PCR

To extract total RNA, the cells were treated with TRIzol reagent (#DP424, Tiangen Biotech) following the manufacturer's instructions. Purified RNA was reverse transcribed into cDNA using PrimeScript™ RT Master Mix (#RR036A, Takara Biomedical Technology). qRT-PCR was then performed using SGExcellFast SYBR Mixture (#B532955-0005, Sangon Biotech) following the

Table 2
Sequence of primers used for ChIP-qPCR.

rDNA region	position	forward	position	reverse
upstream	−988	GCTTCTCGACTCACGGTTTC	−798	GGAGCTCTGCCTAGCTCACA
upstream	−410	GATCCTTTCTGGCGAGTCC	−272	GGAGCCGGAAGCATTTTC
promoter	−48	GAGGTATATCTTTCGCTCCGAGTC	−14	CAGCAATAACCCGGCGG
promoter	−46	GGTATATCTTTCGCTCCGAG	13	AGCGCAGGTCGCCAGAGGA
18S	4013	AAACGGCTACCACATCCAAG	4148	CCTCCAATGGATCCTCGTTA
28S	10,319	GAACTTTGAAGCCGAAGTG	10,450	ATCTGAACCCGACTCCCTTT
IGS	18,499	TGGTGGGATTGGTCTCTCTC	18,572	CAGCCTGCGTACTGTGAAAA

standard reaction conditions on the Roche LightCyclerR 480 Quantitative PCR System (Indianapolis, IN, USA). The following primers were used: pre-rRNA (forward GCTGACACGCTGTCTCTG, reverse TCGGACGCGGAGAGAAC), c-MYC (forward GGCTCCTGGCAAAGGTCA, reverse CTGCGTAGTTGTGCTGATGT), β -actin (forward: AGAGCTACGAGCTGCCTGAC, reverse: AGCACTGTGTTGGCGTACAG), 5' ETS rRNA (forward: GCTGACACGCTGTCTCTCTG, reverse: ACGCGGAGAGAACAGCAG). The relative expression of the target RNA was calculated using the $2^{-\Delta\Delta C_t}$ method and normalized by the level of the housekeeping gene β -actin.

2.16. RNA immunoprecipitation (RIP) assay

Firstly, the gastric cancer cells were harvested, with optional treatment of cells with formaldehyde to cross-link *in vivo* protein-RNA complexes. Then nuclei were isolated, nuclear pellets were lysed and Chromatin was sheared. The RNA binding protein (RBP) of interest was then immunoprecipitated together with the bound RNA, and the unbound material was washed off. The RNA bound to the immunoprecipitated RBP was purified, and then reverse transcribed into cDNA which was subsequently analyzed by qPCR.

2.17. Tumor xenograft

For tumor xenograft experiments, MKN-45 cells (3×10^6 cells/mouse) transduced with lentivirus containing Tet-shRNA targeting TAF1B were mixed with 100 μ L of serum-free culture medium and subcutaneously injected into 8 male BALB/c mice. Starting from the 3rd week after tumor implantation to induce shRNA expression, the mice were randomly divided into two groups: one group was treated with doxycycline (10 mg/kg/day), while the other group was treated with saline. Tumor size was measured every 5 days for 20 days using a digital caliper, and tumor volume was calculated using the formula: tumor volume = (Width [2] \times Length)/2. The mice were euthanized once the largest tumor volume exceeded 800 mm³. The tumor burdens were weighed and processed for further evaluation.

2.18. Bioinformatic analysis

The expression levels of TAF1B in human patients' samples were analyzed using the web-based tool Gene Expression Profiling Interactive Analysis (GEPIA, <http://gepia.cancer-pku.cn>) and TCGA data. Statistical significance was determined based on a log-rank p-value of <0.05.

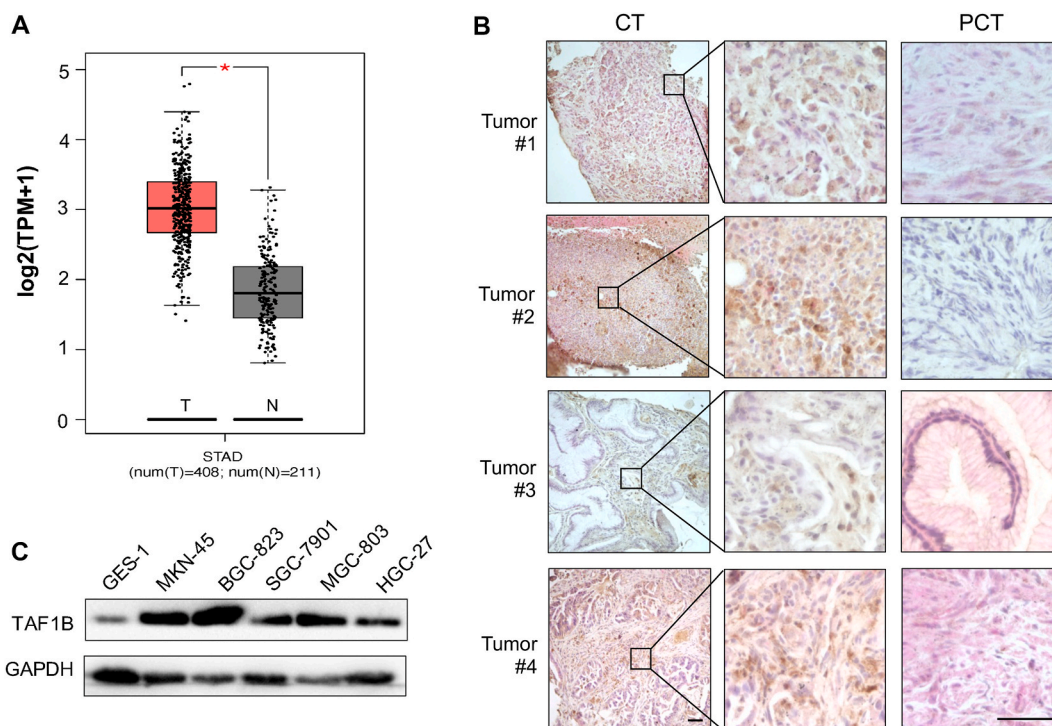


Fig. 1. TAF1B is overexpressed in STAD. (A) The mRNA expression of TAF1B was analyzed using the web-based tool GEPIA. T, tumor sample; N, normal tissue. *, $P < 0.05$. (B) Expression of TAF1B in gastric gland tissue of patients with gastric cancer. Scale bar represents 50 μ m. CT: cancerous tissue; PCT: paracancerous tissue. (C) TAF1B was highly expressed in STAD cancer cell lines. GES-1 is a normal gastric epithelium cell line.

2.19. Statistical analysis

Statistical analyses were performed using the IBM SPSS Statistics [26] software (Armonk, NY, USA). Student's two-tailed *t*-test or two-way ANOVA was used for value calculation. The *p* values were expressed as **p* < 0.05, ***p* < 0.01, and NS for no statistical significance.

3. Results

3.1. *TAF1B* is overexpressed in STAD patients and gastric carcinoma cell lines

We investigated the role of *TAF1B* in STAD progression. Analysis of The Cancer Genome Atlas (TCGA) data showed that *TAF1B* expression was significantly higher in gastric cancer tissues compared to normal gastric tissues (Fig. 1A). Most components of the RNA polymerase I machinery were also upregulated in STAD, including the two largest subunits. However, only *TAF1B* expression was significantly higher in our own data (not shown). Immunohistochemistry staining revealed that *TAF1B* staining intensity was significantly greater in tumor tissues than in adjacent normal tissues (Fig. 1B). Western blot analysis demonstrated higher *TAF1B* protein levels in gastric cancer cell lines relative to the normal gastric epithelial cell line GES-1 (Fig. 1C). These findings indicate that *TAF1B* is overexpressed in STAD and may play a role in gastric tumorigenesis, suggesting it warrants further investigation as a potential therapeutic target.

3.2. Depletion of *TAF1B* inhibits the proliferation of gastric cancer cells

We next investigated the role of *TAF1B* in gastric cancer cell survival. Two different short-hairpin RNAs (shTAF1B#2 and shTAF1B#6) were selected based on their efficacy in knocking down *TAF1B* expression. *TAF1B* knockdown significantly inhibited the growth of two STAD cell lines SGC-7901 and MKN-45 (Fig. 2A, S1A).

Additionally, we observed a reduction in the formation of anchorage-dependent colonies in SGC-7901 and MKN-45, which was shown by decreased colony numbers and sizes (Fig. 2B, S1B). To exclude off-target effects, a rescue experiment was performed by re-expressing shRNA-resistant full-length *TAF1B* in cells expressing shTAF1B#6. Cell growth and colony formation were significantly recovered (Fig. 2C and D). Moreover, a significant reduction of Ki67 and EdU staining of the nucleus of SGC cells following *TAF1B* knockdown, suggesting decreased gastric cancer cell proliferation (Fig. 2E and F). Cell cycle analysis by PI staining showed that *TAF1B* knockdown led to cell cycle arrest with an increased G1 population and decreased S and G2/M populations (Fig. 2G, S1C).

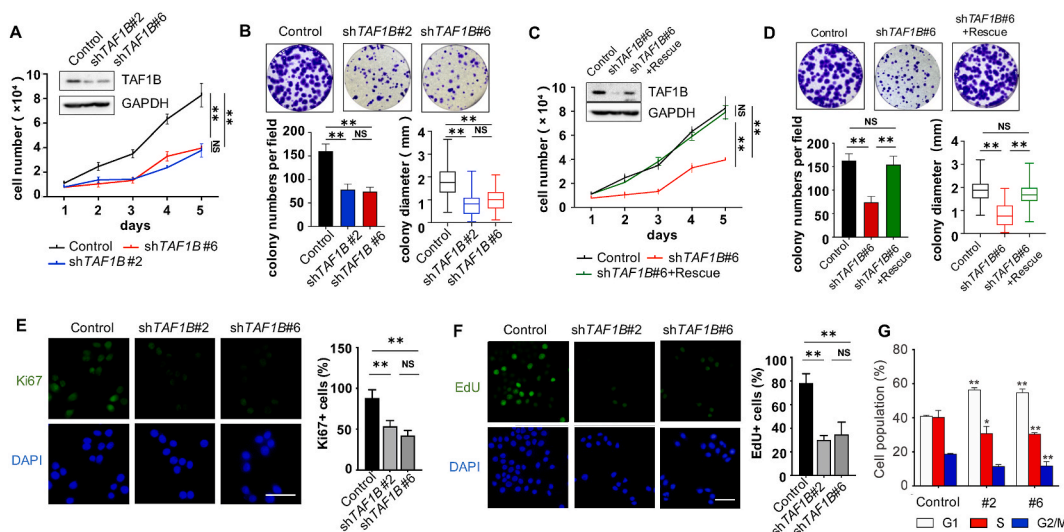


Fig. 2. Depletion of *TAF1B* inhibits proliferation and survival of gastric cancer cells. SGC-7901 cells were stably transduced with lentiviruses containing expressing vectors of either control or *TAF1B* shRNAs (#2 and #6). The cell lysates were collected 3 days after transduction. (A) SGC-7901 cells were counted for 4 days after seeding. Upper left, Western blot analysis shows *TAF1B* knockdown efficiency. Lower left, cell growth curves of SGC-7901 cells. (B) The representative images of colony formation assays. Lower, colony numbers and diameters per field were calculated for at least 3 fields. (C) Rescue assay of *TAF1B* in SGC-7901 cells. Upper left, the examination of knockdown and re-expression of *TAF1B* in cells by western blotting. Cell growth curves were measured for 4 days. (D) The colonies were stained and photographed 14 days after seeding, the numbers and diameters per field were calculated for at least 3 fields. (E, F) The representative images of immunochemical staining with Ki67 (cell proliferation marker) and EdU (detect DNA synthesis) in SGC-7901 cells transduced with scramble or *TAF1B* shRNAs (#2 and #6), respectively. Scale bar represents 50 μ m. Right, quantification of Ki67 and EdU positive cells (*n* = 3). (G) Cell cycle distribution after *TAF1B* knockdown. Data are shown as means \pm SD (*n* = 3). *, *P* < 0.05; **, *P* < 0.01; NS, no significance.

Since cell cycle arrest could induce cell senescence [23]; we next examined cellular senescence in gastric cancer cells following *TAF1B* knockdown. However, β -galactosidase staining was not increased in MKN-45 and SGC-7901 cells after *TAF1B* depletion (Fig. S2A). In addition, the level of p16 protein, a well-established marker of cell senescence [24], was not significantly altered after *TAF1B* knockdown (Fig. S2B). In summary, *TAF1B* knockdown inhibited the growth and proliferation of gastric cancer cells, likely at least partly by inducing cell cycle arrest. However, the effects do not appear to be mediated by cellular senescence, as senescence markers were unchanged after *TAF1B* depletion.

3.3. Deprivation of *TAF1B* inhibits growth of MKN-45 cell-derived STAD *in vivo*

We investigated the effect of *TAF1B* knockdown on gastric tumor growth *in vivo*. We established MKN-45 cell lines stably expressing a doxycycline-inducible *TAF1B* shRNA. Successful doxycycline-induced *TAF1B* knockdown was confirmed by Western blot (Fig. 3A). Three weeks after injecting these cells into nude mice, doxycycline was administered to induce shRNA expression. Mice were euthanized after six weeks and the tumors were harvested. The results, as shown in Fig. 3B and C, demonstrate that *TAF1B* knockdown significantly impeded the growth of MKN-45 cell-derived tumors in mice. Furthermore, immunohistochemical staining of Ki67, a marker of cell proliferation, was reduced in tumors with *TAF1B* deficiency (Fig. 3D). These findings indicate that *TAF1B* knockdown impairs gastric tumor growth *in vivo*, likely by inhibiting cell proliferation.

3.4. Depletion of *TAF1B* impairs the interaction of PIC components and causes dissociation of Pol I from rDNA

TAF1B is a crucial component of the PIC (Fig. S3). Interestingly, our analysis showed that the content of most other PIC components remained unchanged after *TAF1B* knockdown, but the Pol I β subunit was substantially reduced (Fig. 4A). To further understand how Pol I β was decreased, we examined the mRNA expression and ubiquitination of Pol I β after *TAF1B* knockdown. Our results indicate that *TAF1B* inhibition reduced Pol I β mRNA expression (Fig. S4A). Immunofluorescent staining using a specific anti-RPA135 (Pol I β) antibody also highlighted a significant reduction in the nuclear localization of Pol I β after *TAF1B* shRNA treatment (Fig. S4B). In addition, we examined the interaction between the various components of the PIC after *TAF1B* depletion. Interestingly, the interaction between *TAF1A* and *TAF1C* or TBP was markedly weakened (Fig. 4B). However, we found that *TAF1B* deficiency had no significant effect on the interaction between *RRN3* and the largest subunit of Pol II (Fig. 4C). Even though, the knockdown of *TAF1B* clearly reduced the interaction between the α and β subunits of Pol II, as shown in Fig. 4D. Moreover, the binding of Pol I α and Pol I β with rDNA

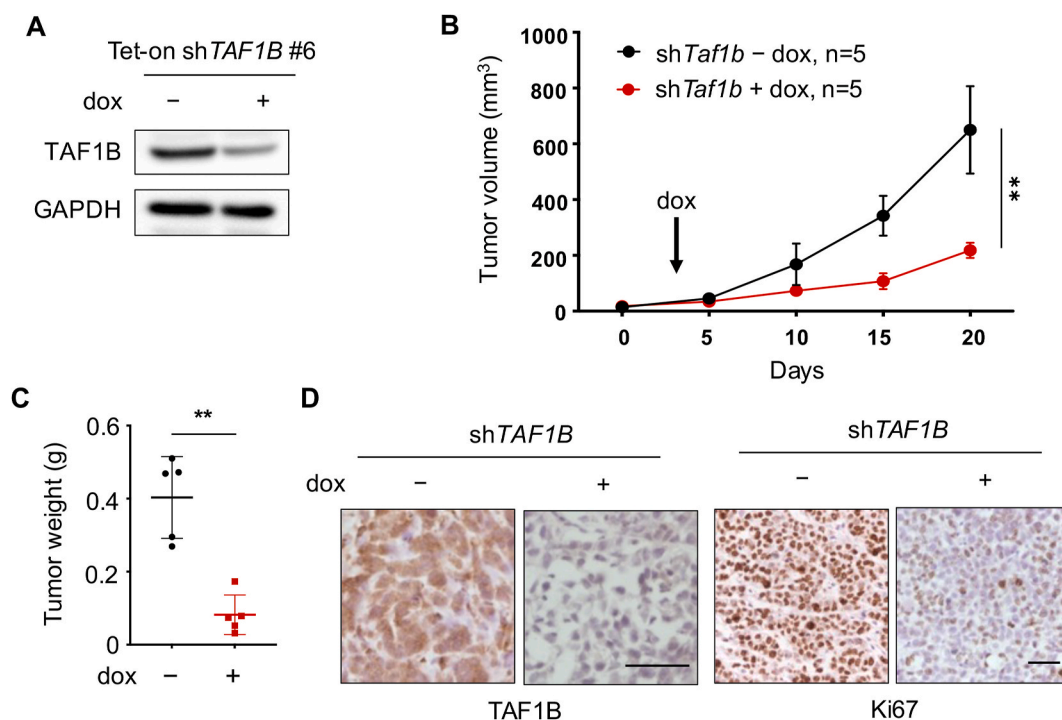


Fig. 3. Deprivation of *TAF1B* inhibits STAD tumor growth *in vivo*. MKN-45 cells expressing doxycycline (Dox)-induced *TAF1B* shRNA were amplified by tissue culture. (A) The efficiency of knockdown after Dox induction was examined. (B) Nude mice implanted with MKN-45 cells received Dox to induce shRNA expression in the 3rd week after the tumor implantation. Tumor volumes (n = 5) were measured by calipers per five days for 20 days. (C) The measurement of weight of dissected tumors (n = 5). (D) The representative images of Ki67 and *TAF1B* immunochemical staining in the tumors. Scale bar represents 20 μ m. Data are shown as means \pm SD (n = 5). **, P < 0.01.

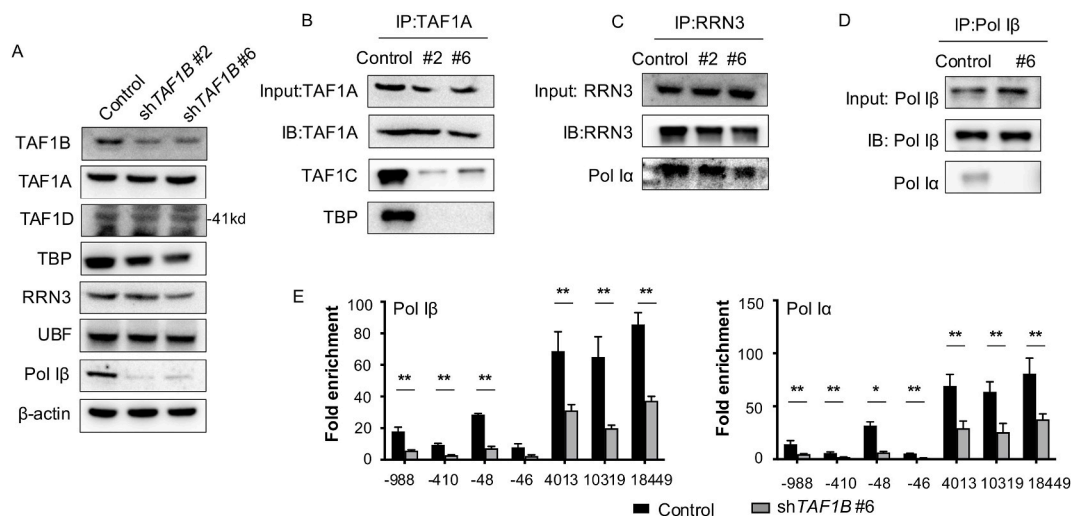


Fig. 4. Deficiency of *TAF1B* disrupts internal interaction of PIC complex and causes dissociation of *Pol II* from rDNA promoters. SGC-7901 cells were stably transduced with lentiviruses containing expressing vectors of either scramble or *TAF1B* shRNAs (#2 and #6). The cell lysates were collected 3 days after transduction. (A) The protein abundance of major components of PIC complex was examined by western blotting after *TAF1B* knockdown. (B) *TAF1A* specific antibody was used to immunoprecipitated endogenous *TAF1A* from SGC-7901 cells lysates with indicated treatment. The binding of *TAF1C* or *TBP* to *TAF1A* was examined by western blotting. (C) *RRN3* specific antibody was used to immunoprecipitated endogenous *RRN3* from SGC-7901 cells lysates with indicated treatment. The binding of *Pol α* to *TAF1A* was examined by western blotting. (D) The interaction of *Pol α* and *Pol β* was immunoprecipitation assay. (E) The binding of RNA polymerase α and β to rDNA was analyzed by ChIP-qPCR. The positions of amplification primers were denoted numerically. Data are shown as means \pm SD (n = 3). *, P < 0.05; **, P < 0.01.

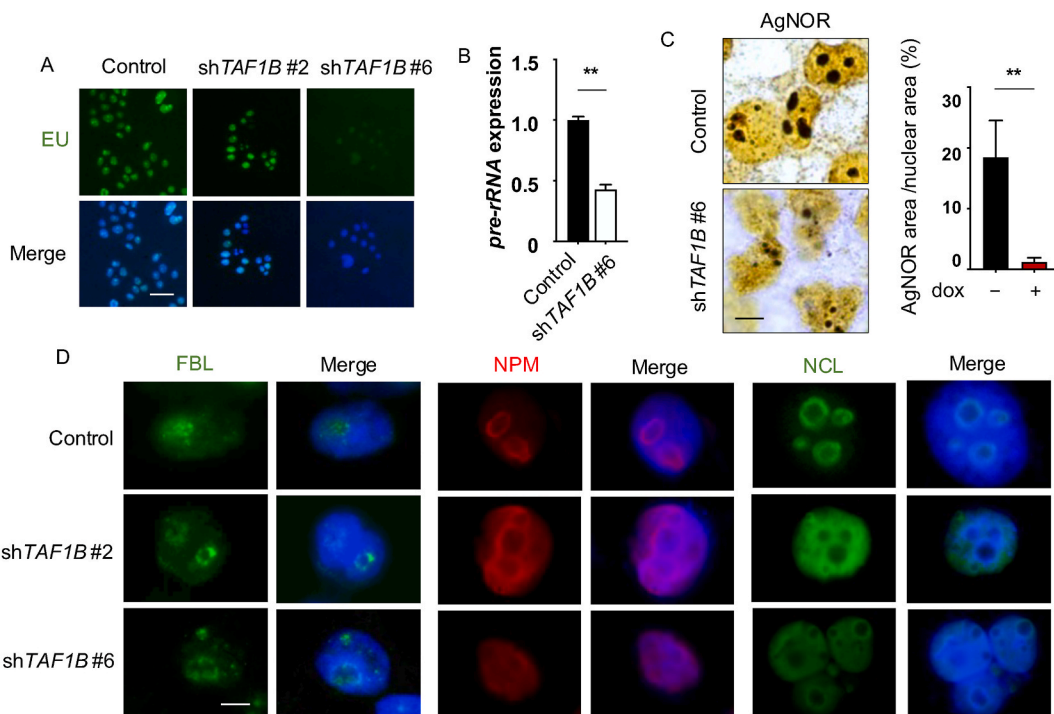


Fig. 5. Knockdown of *TAF1B* represses rRNA synthesis and causes segregation of nucleolar proteins. SGC-7901 cells were stably transduced with lentiviruses containing expressing vectors of either control or *TAF1B* shRNAs (#2 and #6). The cell lysates were collected 3 days after transduction. (A) De novo rRNA synthesis in SGC-7901 cells was measured by EU labeling. Scale bar represents 50 μ m. (B) The mRNA expression of pre-rRNA was determined by qRT-PCR (n = 3). Data are shown as means \pm SD. *, P < 0.05; **, P < 0.01. (C) The representative images from the silver staining for argyrophilic nucleolar organizer region-associated proteins (AgNORs). Scale bar represents 5 μ m. Right, quantitation of AgNORs area for at least 5 fields. (D) Knockdown of *TAF1B* induced redistribution of fibrillarlin (FBL), nucleophosmin (NPM) and nucleolin (NCL). Scale bar represents 5 μ m.

promoters was notably weakened (Fig. 4E). Overall, these findings suggest that *TAF1B* knockdown negatively impacts the function of *PoII* by inhibiting its mRNA expression, reducing its nuclear localization and weakening its interactions with other PIC components.

3.5. Deficiency of *TAF1B* represses rRNA synthesis and causes segregation of nucleolar proteins

To further assess the impact of *TAF1B* knockdown on RNA synthesis and rRNA transcription in STAD cells, we treated the cells with 5-Ethynyl Uridine (EU) to label newly synthesized RNA. We found a significant decrease in EU staining after *TAF1B* gene knockdown (Fig. 5A). Additionally, we observed a decrease in the transcription of precursor rRNA (47S pre-rRNA) and 5' external transcribed spacer rRNA (5' ETS rRNA) after *TAF1B* knockdown (Fig. 5B and S5A). Argrophilic proteins are known to be involved in rRNA transcription and processing, and the number of AgNORs (argrophilic proteins in the nucleolus organizer region) is closely associated with rRNA transcriptional activity[25]. In xenograft tumors with doxycycline-inducible *TAF1B* knockdown, AgNOR staining was significantly decreased, indicating reduced rRNA transcription *in vivo* (Fig. 5C). Inhibiting rRNA synthesis can disrupt the nucleolar structure and redistribute nucleolar proteins [26–28]. Fibrillarin (FBL), a marker of new nucleolus formation [29], formed more distinct foci after *TAF1B* depletion (Fig. 5D). However, the distribution of nucleophosmin, another nucleolar protein, did not show a significant change after *TAF1B* deprivation in STAD cells did not show a significant change after *TAF1B* deprivation (Fig. S5B).

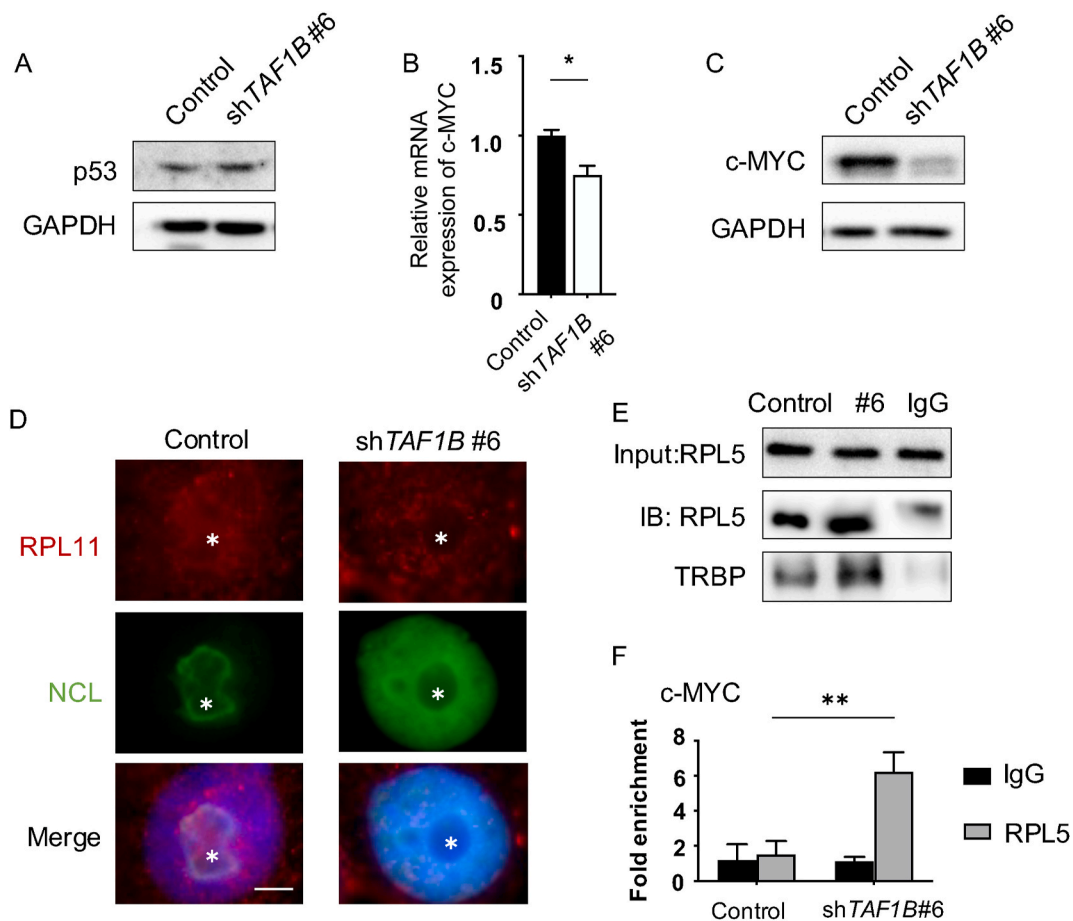


Fig. 6. Knockdown of *TAF1B* inactivates c-MYC. MKN-45 cells were stably transduced with lentiviruses containing expressing vectors of either control or *TAF1B* shRNAs. The cell lysates were collected 3 days after transduction. (A) The amount of p53 protein were examined by western blotting after *TAF1B* knockdown. (B) The expression of c-MYC mRNA was determined by qRT-PCR (n = 3). (C) The amount of c-MYC protein were examined by western blotting after *TAF1B* knockdown. (D) Knockdown of *TAF1B*-induced redistribution of *RPL11* and nucleolin (NCL). Asterisks, cap structures. Scale bar represents 5 μ m. (E) *RPL5* specific antibody was used to immunoprecipitated endogenous *RPL5* from MKN-45 cells lysates with indicated treatment. The binding of *TRBP* to *RPL5* was examined by western blotting. (F) Relative enrichment of *RPL5* with c-MYC mRNA was determined by RNA immunoprecipitation from MKN-45 cells lysates with indicated treatment. Ct values of each RIP reaction were normalized to input fractions to obtain Δ Ct, and c-MYC fold-enrichment represent $\Delta\Delta$ Ct values derived from normalized Δ Ct values of *RPL5* and IgG RIPs at each treatment (n = 3). Data are shown as means \pm SD. *, P < 0.05; **, P < 0.01.

3.6. Knockdown of *TAF1B* down-regulates *c-MYC* through enhancing mRNA degradation

As stated earlier, *TAF1B* knockdown induced marked nucleolar stress in STAD cells. Nucleolar stresses lead to cell cycle arrest, cellular senescence, or apoptosis through p53 dependent or independent signaling pathways [30,31]. We explored the involvement of p53 in *TAF1B*-associated phenotypes by western blotting to determine p53 expression levels. The results showed that following *TAF1B* knockdown, the quantity of p53 remained unaltered (Fig. 6A), indicating the effects of *TAF1B* was p53-independent. *c-MYC* is a vital regulator of cell cycle progression, and its expression is closely linked to cell proliferation. Nucleolar stress response is known to promote mRNA and protein degradation of *c-MYC* [32]. Indeed, our results revealed that mRNA expression and protein abundance of *c-MYC* were reduced after *TAF1B* knockdown (Fig. 6B and C). Ectopic expression of *c-MYC* in STAD cells partially rescued the proliferation defect induced by *TAF1B* knockdown (Fig. S6). Upon nucleolar stresses, ribosomal proteins *RPL5* and *RPL11* are released from nucleoli to nuclei, where they bind to the 3' untranslated region (3' UTR) of *c-MYC* mRNA and accelerate its degradation by RNA-induced silencing complex (RISC) [32–34]. We observed the alteration of nuclear distribution of *RPL11* after *TAF1B* depletion (Fig. 6D). Furthermore, the interaction of *RPL5* and *TRBP*, a major component of RISC, was strengthened (Fig. 6E). Additionally, the RNA immunoprecipitation assay revealed an increase in *c-MYC* mRNA enrichment of *RPL5* after *TAF1B* knockdown, suggesting enhanced RISC assembly in *c-MYC* mRNA degradation in STAD cells (Fig. 6F).

4. Discussion

In the PIC, *SL1* confers specificity for RNA polymerase I transcription through its TBP-associated factors (TAFs), including *TAF1B*, *TAF1A*, *TAF1C*, *TAF1D*, and *TAF12*, which were specific for RNA polymerase I [35]. *TAF1B* has been shown to interact directly not only with *RRN3* and rDNA promoter [15–18], but also to stabilize the structure of *SL1* [19]. Our study found that *TAF1B* knockdown induced nucleolar stress, inhibited proliferation in gastric cancer cells and likely acts through p53-independent pathways to affect downstream effectors involved in ribosome biogenesis and cell growth.

Our findings also suggest that *TAF1B* knockdown-induced nucleolar stress activates a *c-MYC* mRNA degradation mechanism. Following nucleolar stress, ribosomal proteins *RPL5* and *RPL11* are released from nucleoli and bind to the 3' UTR of *c-MYC* mRNA, targeting it for degradation. In addition to their canonical role in ribosomal biogenesis, ribosomal proteins (RP) also function as sensors of cellular stress, regulate mRNA stability and cell growth and proliferation regulation [36]. *RPL5* and *RPL11*, which are synthesized by the large subunit of ribosome 60S, can not only maintain the stability of p53 protein [37], but also inhibit *MYC* transcription [34,38]. Inhibition of *RiBi* function resulted in decreased RP content in nucleoli and increased RP content in the nucleus plasma, thereby providing conditions for RP to perform its extra-ribosomal functions (Fig. 6D). *RPL11* can reduce *c-MYC* content through two mechanisms. First, an increase in *RPL11* content can directly inhibit *c-MYC* activity through negative feedback [38]. However, this mechanism was excluded in our study, as there was no significant increase in *RPL11* content, but rather in *RPL5* in gastric cancer cells following *TAF1B* knockdown (Fig. S7). Second, *RPL11* and *RPL5* in combination with RNA-induced silencing complex (RISC) can degrade *c-MYC* mRNA transcription, leading to a reduction in the amount of *c-MYC* protein [32–34]. Through a series of subsequent experimental tests (Fig. 6E and F), we have confirmed that the second mechanism plays a role in STAD after *TAF1B* knockdown.

Furthermore, *c-MYC* has been shown to bind to the E-box of the *Pol I β* promoter to regulate *Pol I β* gene transcription [39]. *Pol I β* , the second largest subunit of *Pol II*, is crucial for transcriptional initiation and is considered to be one of the PIC components [40]. Importantly, we observed a reduction in both *Pol I β* transcription and protein levels (Fig. 4A, S4A) following *TAF1B* knockdown. As *Pol I β* plays a critical role in specific transcriptional initiation, its decrease may contribute to the inhibitory effect of *TAF1B* knockdown on cell growth and proliferation [41,42]. The inhibitory effect of *TAF1B* gene knockdown on STAD growth and proliferation may be a co-effect of *c-MYC* and *Pol I β* , although further experiments are necessary to determine which aspect plays the dominant role, or whether both play equally important roles. Understanding the mechanism in this aspect could provide novel ideas for selecting STAD therapeutic targets, and provide an early theoretical basis for clinical STAD treatment.

One limitation of our current work is that *TAF1B* knockdown experiments were only performed in STAD cell lines. It remains unclear whether the inhibitory effects of *TAF1B* depletion are prevalent in other cancer types. We investigated the expression level of *TAF1B* in a variety of cancers using data from TCGA. It showed that *TAF1B* was up-regulated in several kinds of tumors (Fig. S8). This finding suggests that upregulation of *TAF1B* expression does not occur exclusively in STAD, nor is it seen in all types of tumors. Also, the importance of *TAF1B* in cancers may vary depending on the specific intracellular signaling pathways involved. Although the importance of *TAF1B* in cancers may be context-dependent, our previous study showed that *TAF1B* has similar effects at least on HCC cells. Furthermore, suppression of *TAF1B* in normal cell lines such as MRC-5 exhibited some unfavorable effects on cell cycle and proliferation, although the effects were less severe than in tumor cells (data not shown). This might be because ribosome synthesis in tumor cells is more vigorous, and *TAF1B* suppression exacerbates the nucleolar stress already present in tumor cells. Another limitation is we have not explored the role of other TAFs in STAD proliferation. Depletion of these TAFs may impair rRNA gene transcription and in turn cell proliferation as well. Further studies of multiple TAF proteins could provide a more comprehensive understanding of their functions and therapeutic potential.

The targeting of *TAF1B* in STAD holds potential clinical implications. One such implication is the therapeutic potential of inhibiting *TAF1B*, which could lead to a slowdown in tumor growth and improved patient outcomes. This is achieved by reducing ribosome biogenesis, a process crucial for the proliferation of cancer cells. Additionally, *TAF1B* expression levels may serve as a biomarker for prognosis and treatment response in STAD patients, allowing for personalized medicine approaches. However, there exist limitations and challenges associated with targeting *TAF1B*. Firstly, *TAF1B* may have other functions beyond its role in ribosome biogenesis, potentially leading to off-target effects and unintended side effects upon inhibition. Secondly, the development of resistance

mechanisms by cancer cells poses a challenge, necessitating the investigation of potential resistance mechanisms that may arise in response to *TAF1B* inhibition. Lastly, the effective delivery of *TAF1B*-targeted therapies specifically to tumor cells, while minimizing off-target effects in normal cells, presents a significant delivery challenge. To translate *TAF1B*-targeted therapy into clinical practice, further research and validation are required. This includes preclinical studies utilizing animal models and clinical trials involving STAD patients to assess the safety, efficacy, and potential side effects of *TAF1B*-targeted therapies. Moreover, the identification of optimal combination therapies or strategies to overcome resistance is crucial for successful clinical implementation.

Funding information

This work was supported by Quzhou Technology Projects [2022K46, 2019K36, 2018K20], Natural Science Foundation of China [81502304], Natural Science Foundation of Zhejiang Province [LQ19H160002], Medical and Health Technology Projects of Zhejiang Province [2017KY696, 2019PY089], Chinese Medicine Science Foundation of Zhejiang Province [2021ZB328].

Ethical statements

The protocols for animal experiments have been reviewed and approved by the Laboratory Animal Management and Ethics Committee of Hangzhou Medical College in Zhejiang Province (license number of animal use permit: SYXK 2023-0032, license number of approval of animal ethical and welfare: ZJCLA-IACUC-202205).

Data availability statements

The authors declare that the data supporting the findings of this study are available within the article and its supplementary information files.

CRediT authorship contribution statement

Hang-fei Chen: Investigation, Conceptualization. **Zhang-ping Li:** Investigation, Formal analysis, Conceptualization. **Qi Wu:** Investigation. **Chun Yu:** Methodology, Formal analysis. **Jing-Yi Yan:** Methodology, Formal analysis. **Yong-feng Bai:** Methodology, Investigation. **Sheng-mei Zhu:** Methodology, Formal analysis. **Mao-xiang Qian:** Writing - review & editing, Writing - original draft, Resources. **Ming Liu:** Writing - review & editing, Resources. **Li-feng Xu:** Supervision, Resources. **Zheng Peng:** Writing - review & editing, Resources. **Feng Zhang:** Writing - review & editing, Writing - original draft, Resources, Project administration, Funding acquisition, Formal analysis, Conceptualization.

Declaration of competing interest

The authors declare that they have no known competing financial interests or personal relationships that could have appeared to influence the work reported in this paper.

Appendix A. Supplementary data

Supplementary data to this article can be found online at <https://doi.org/10.1016/j.heliyon.2023.e23167>.

References

- [1] F. Bray, et al., Global cancer statistics 2018: GLOBOCAN estimates of incidence and mortality worldwide for 36 cancers in 185 countries, *CA Cancer J Clin* 68 (6) (2018) 394–424.
- [2] J. Hooi, et al., Global Prevalence of *Helicobacter pylori* Infection: Systematic Review and Meta-analysis, *Gastroenterology* 153 (2) (2017) 420–429.
- [3] H. Kim, et al., Effectiveness of gastric cancer screening on gastric cancer incidence and mortality in a community-based Prospective Cohort, *Cancer Res Treat* 50 (2) (2018) 582–589.
- [4] C. Hamashima, et al., A community-based, case-control study evaluating mortality reduction from gastric cancer by endoscopic screening in Japan, *PLoS One* 8 (11) (2013), e79088.
- [5] J.K. Jun, et al., Effectiveness of the Korean National cancer screening Program in Reducing gastric cancer mortality, *Gastroenterology* 152 (6) (2017) 1319–1328.e7.
- [6] M. Arnold, et al., Is gastric cancer becoming a rare disease? A global assessment of predicted incidence trends to 2035, *Gut* 69 (5) (2020) 823–829.
- [7] G. Donati, L. Montanaro, M. Derenzini, Ribosome biogenesis and control of cell proliferation: p53 is not alone, *Cancer Res.* 72 (7) (2012) 1602–1607.
- [8] J. Pelletier, G. Thomas, S. Volarevic, Ribosome biogenesis in cancer: new players and therapeutic avenues, *Nat. Rev. Cancer* 18 (1) (2018) 51–63.
- [9] S. Sharifi, H. Bierhoff, Regulation of RNA polymerase I transcription in development, disease, and aging, *Annu. Rev. Biochem.* 87 (2018) 51–73.
- [10] V.L. Nunez, et al., New Roles for the nucleolus in Health and disease, *Bioessays* 40 (5) (2018), e1700233.
- [11] A. Khot, et al., First-in-Human RNA polymerase I transcription Inhibitor CX-5461 in Patients with Advanced Hematologic cancers: Results of a Phase I Dose-Escalation study, *Cancer Discov.* 9 (8) (2019) 1036–1049.
- [12] A. Maiser, et al., Super-resolution in situ analysis of active ribosomal DNA chromatin organization in the nucleolus, *Sci. Rep.* 10 (1) (2020) 7462.
- [13] M. Pils, C. Engel, Structural basis of RNA polymerase I pre-initiation complex formation and promoter melting, *Nat. Commun.* 11 (1) (2020) 1206.

- [14] J.K. Friedrich, et al., TBP-TAF complex SL1 directs RNA polymerase I pre-initiation complex formation and stabilizes upstream binding factor at the rDNA promoter, *J. Biol. Chem.* 280 (33) (2005) 29551–29558.
- [15] A.H. Cavanaugh, et al., Rm3 phosphorylation is a regulatory checkpoint for ribosome biogenesis, *J. Biol. Chem.* 277 (30) (2002) 27423–27432.
- [16] X. Yuan, et al., Multiple interactions between RNA polymerase I, TIF-IA and TAF(I) subunits regulate preinitiation complex assembly at the ribosomal gene promoter, *EMBO Rep.* 3 (11) (2002) 1082–1087.
- [17] U. Rudloff, et al., TBP-associated factors interact with DNA and govern species specificity of RNA polymerase I transcription, *EMBO J.* 13 (11) (1994) 2611–2616.
- [18] H. Beckmann, et al., Coactivator and promoter-selective properties of RNA polymerase I TAFs, *Science* 270 (5241) (1995) 1506–1509.
- [19] S. Naidu, et al., TAF1B is a TFIIB-like component of the basal transcription machinery for RNA polymerase I, *Science* 333 (6049) (2011) 1640–1642.
- [20] S. Gupta, et al., Whole Exome-Trio analysis Reveals rare Variants associated with Congenital Pouch Colon, *Children* 10 (5) (2023).
- [21] M. Kloor, et al., A Frameshift Peptide Neoantigen-based Vaccine for Mismatch Repair-Deficient cancers: a Phase I/IIa Clinical Trial, *Clin. Cancer Res.* 26 (17) (2020) 4503–4510.
- [22] H.F. Chen, et al., TAF1B depletion leads to apoptotic cell death by inducing nucleolar stress and activating p53-miR-101 circuit in hepatocellular carcinoma, *Front. Oncol.* 13 (2023), 1203775.
- [23] R. Kumari, P. Jat, Mechanisms of Cellular senescence: cell cycle arrest and senescence associated Secretory Phenotype, *Front. Cell Dev. Biol.* 9 (2021), 645593.
- [24] M.V. Blagosklonny, Cell cycle arrest is not yet senescence, which is not just cell cycle arrest: terminology for TOR-driven aging, *Aging (Albany NY)* 4 (3) (2012) 159–165.
- [25] M. Derenzini, The AgNORs, *Micron* 31 (2) (2000) 117–120.
- [26] S. Boulon, et al., The nucleolus under stress, *Mol Cell* 40 (2) (2010) 216–227.
- [27] D. Hernandez-Verdun, Nucleolus: from structure to dynamics, *Histochem. Cell Biol.* 125 (1–2) (2006) 127–137.
- [28] T. Pederson, The nucleolus, *Cold Spring Harb Perspect Biol* 3 (3) (2011).
- [29] R.L. Ochs, et al., Fibrillarin: a new protein of the nucleolus identified by autoimmune sera, *Biol Cell* 54 (2) (1985) 123–133.
- [30] K. Yang, J. Yang, J. Yi, Nucleolar Stress: hallmarks, sensing mechanism and diseases, *Cell Stress* 2 (6) (2018) 125–140.
- [31] A. Russo, G. Russo, Ribosomal proteins control or Bypass p53 during nucleolar stress, *Int. J. Mol. Sci.* 18 (1) (2017).
- [32] K.B. Challagundla, et al., Ribosomal protein L11 recruits miR-24/miRISC to repress c-Myc expression in response to ribosomal stress, *Mol. Cell Biol.* 31 (19) (2011) 4007–4021.
- [33] H.C. Lee, et al., RNA polymerase I Inhibition with CX-5461 as a Novel therapeutic Strategy to Target MYC in Multiple Myeloma, *Br. J. Haematol.* 177 (1) (2017) 80–94.
- [34] J.M. Liao, et al., Ribosomal proteins L5 and L11 co-operatively inactivate c-Myc via RNA-induced silencing complex, *Oncogene* 33 (41) (2014) 4916–4923.
- [35] L. Comai, et al., Reconstitution of transcription factor SL1: exclusive binding of TBP by SL1 or TFIID subunits, *Science* 266 (5193) (1994) 1966–1972.
- [36] J. Kang, et al., Ribosomal proteins and human diseases: molecular mechanisms and targeted therapy, *Signal Transduct Target Ther* 6 (1) (2021) 323.
- [37] S. Bursac, et al., Mutual protection of ribosomal proteins L5 and L11 from degradation is essential for p53 activation upon ribosomal biogenesis stress, *Proc Natl Acad Sci U S A* 109 (50) (2012) 20467–20472.
- [38] M.S. Dai, et al., Inhibition of c-Myc activity by ribosomal protein L11, *EMBO J.* 26 (14) (2007) 3332–3345.
- [39] G. Poortinga, et al., c-MYC coordinately regulates ribosomal gene chromatin remodeling and Pol I availability during granulocyte differentiation, *Nucleic Acids Res.* 39 (8) (2011) 3267–3281.
- [40] G. Miller, et al., hRRN3 is essential in the SL1-mediated recruitment of RNA Polymerase I to rRNA gene promoters, *EMBO J.* 20 (6) (2001) 1373–1382.
- [41] F. Yang, et al., POLR1B is upregulated and promotes cell proliferation in non-small cell lung cancer, *Oncol. Lett.* 19 (1) (2020) 671–680.
- [42] X. Wang, et al., Long non-coding RNA ZFAS1 promotes colorectal cancer tumorigenesis and development through DDX21-POLR1B regulatory axis, *Aging (Albany NY)* 12 (22) (2020) 22656–22687.